Probing Quantum Plasmon Coupling Using Gold Nanoparticle Dimers with Tunable Interparticle Distances Down to the Subnanometer Range

Hoon Cha,[†] Jun Hee Yoon,[†] and Sangwoon Yoon[*]

Department of Chemistry, Dankook University, 152 Jukjeon-ro, Suji-gu, Yongin, Gyeonggi 448-701, Korea. [†]These authors contributed equally.

ABSTRACT The assembly of noble metal nanoparticles is an appealing means to control the plasmonic properties of nanostructures. Dimers are particularly interesting because they are a model system that can provide fundamental insights into the interactions between nanoparticles in close proximity. Here, we report a highly efficient and facile assembly method for dimers and other forms of assemblies. Gold nanoparticles (AuNPs) adsorbed on aminosilanized glass surfaces protect the silanes underneath the nanoparticles from hydrolysis. This *masked* desilanization allows us to prepare AuNP homodimers on glass slides with remarkably high yield (~90%). The interparticle distance and, accordingly, the surface plasmon coupling are readily tuned at the molecular level using self-assembled monolayers of alkanedithiols. As the interparticle distance is reduced, the resonance surface plasmon coupling progressively redshifts, following the classical electromagnetic model. When the interparticle distance enters the subnanometer regime, however, the resonance band begins to blueshift and significantly broadens. The comparison of our observations with theoretical studies reveals that quantum tunneling effects play a significant role in the plasmonic response of AuNP dimers in the subnanometer gap region. The assembly method based on the masked desilanization is extendable to the formation of various other forms of nanoassemblies and, thus, will further our understanding of plasmonic interactions in nanoassemblies.

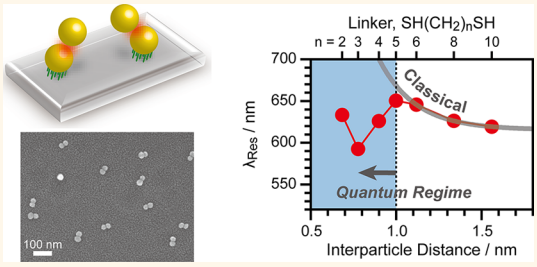

KEYWORDS: plasmonics · surface plasmon coupling · quantum plasmonics · charge transfer plasmon · nanoparticle dimer · desilanization

Surface plasmon resonance (SPR) is the defining property of noble metal nanoparticles.[1] Excitation of collective oscillations of the conduction electrons (called surface plasmons) at the resonance wavelength leads to significant light scattering, the generation of local electromagnetic fields around the nanoparticles, and localized heat release by the nanoparticles.[2] These properties facilitate a wide variety of applications involving noble metal nanoparticles including chemosensing,[3] biological imaging,[4] solar energy conversion,[5] and cancer cell treatment.[6] Therefore, the production and control of the SPR is at the heart of plasmonics.

The SPR can be controlled by modifying individual nanoparticles. The resonance wavelength varies with the size, shape, materials, and local environment of the nanoparticles.[7] Therefore, the synthesis of nanoparticles with different structures or compositions leads to the changes in the resonance wavelength. An alternative to cumbersome synthetic procedures is to use preformed nanoparticles as building blocks and assemble them into a new structure.[8] When the nanoparticles are in close proximity, the individual surface plasmons can couple, leading to a shift in the optical response.[9] Surface plasmon coupling sensitively depends on the way the nanoparticles are assembled. Therefore, variations in the assembly parameters (interparticle distance, configuration, the number of nanoparticles, *etc.*) and permutations in the constituent nanoparticles (size, shape, materials, *etc.*) allow one to finely tune the resonance wavelength. Furthermore, nanoassemblies act as excellent nanoantennas for plasmonics studies because the electromagnetic fields generated by the surface plasmons are highly focused at interstitial sites.[10] Therefore, the abundant nanogaps present

* Address correspondence to sangwoon@dankook.ac.kr.

Received for review June 15, 2014 and accepted August 4, 2014.

Published online August 04, 2014
10.1021/nn5032438

in nanoassemblies provide hot spots for many near-field enhancement effects such as surface-enhanced Raman scattering, surface-enhanced fluorescence, and plasmonic photocatalytic activities.[5,11−13]

Controlling the resonance wavelength using nanoparticle assemblies requires a fundamental understanding of surface plasmon coupling. Many experimental observations have indicated that when surface plasmons are coupled, a new band appears at a longer wavelength than the SPR band of isolated nanoparticles.[14−19] The surface plasmon coupling band further redshifts as the interaction among the nanoparticles strengthens. This phenomenon is explained in the framework of classical electrodynamics. In a simple but intuitive surface plasmon hybridization model, interactions between nanoparticles create a new hybridized bonding mode, similar to a bonding orbital in molecular orbital theory.[20,21] This resonance is redshifted with respect to the SPR mode of individual nanoparticles. When two particles interact more strongly as the interparticle distance decreases, the bonding mode is lowered in energy and, thus, the resonance wavelength further redshifts. The quantitative relationship between the redshift of the surface plasmon coupling band and the interparticle distance yields a plasmon ruler equation that allows one to measure interparticle distances from optical spectra with great accuracy.[16,17,22−24]

This simple classical electrodynamics model, however, breaks down as the interparticle distance enters the subnanometer regime. Theoretical studies by Nordlander and co-workers revealed that tunneling effects begin to disturb the interaction between the surface plasmons when the interparticle distance is below 1 nm.[25,26] Their quantum mechanical calculations showed that the gradual redshift of the plasmon coupling band with decreasing interparticle distance transitions to a blueshift as quantum effects begin to dominate the interaction. Despite theoretical predictions and commonly accepted notions, experimental evidence for these quantum effects in coupled nanoparticles has rarely been presented.[27−30]

For comparison with quantum calculations, plasmon coupling must be measured on dimers as a function of the interparticle distance. However, it is challenging to prepare nanoparticle dimers with controllable interparticle distances down to the subnanometer range in high yield. Top-down methods, such as electron beam lithography, produce arrays of well-controlled nanodisc dimers, but with the interparticle distance usually limited to >2 nm due to electron dispersion.[16] Bottom-up approaches using molecular linkers are better suited to finely controlling the interparticle distance. In this process, however, stoichiometric mixing of nanoparticles functionalized with linkers inevitably leads to a mixture of assemblies with undesired multimers and unlinked monomers.[18,31−35] The required postassembly separation process using electrophoresis or density-gradient centrifugation significantly lowers the overall yield of the dimers and often destabilizes the product. The spatially selective functionalization of nanoparticles permits more controlled assembly.[36−41] However, the interparticle distance is mostly longer than 2 nm because DNA hybridization or amide bond formation used to connect nanoparticles requires a certain length for the linkers.

Recently, we developed a new assembly method to prepare core−satellite nanoassembly structures with near 100% yield.[42] The core-to-satellite interparticle distance was controlled at the molecular level down to ~0.7 nm using self-assembled monolayers (SAMs) of alkanedithiols. The combination of the ultrahigh purity of the assemblies and the tunable interparticle distance allowed us to measure the surface plasmon coupling as a function of the interparticle distance. In particular, we discovered strong evidence of quantum effects in the Ag core−Au satellite assemblies with gap distances less than 1 nm.[28] However, direct comparison with quantum mechanical calculations was unfeasible due to the large size and complexity of the assembly structure. Therefore, a new assembly method for dimers with controllable interparticle distances is highly desired.

In this article, we report a new assembly method that prepares dimers with ~90% yield. The realization of high-purity dimers with tunable interparticle distances inspired us to measure quantum effects at subnanometer interparticle distances. This paper presents three research outcomes. We first report our observation of a novel phenomenon that we named *masked desilanization*, which provides a solid foundation for the newly developed assembly method. Next, we describe the procedure and the important results of the new assembly method for homodimers. We also demonstrate that this method is not limited to the assembly of homodimers, but is highly extendable to the assembly of other forms of clusters. Finally, we discuss the quantum effects observed in the optical response of the dimers with subnanometer interparticle distances.

RESULTS AND DISCUSSION

Observation of Masked Desilanization. Our new assembly method is based on building up nanoparticles one after another on a solid support. The key element in this process is masked desilanization. Figure 1 outlines the general desilanization and the newly observed masked desilanization. Desilanization generally involves the hydrolysis of the siloxane bond under basic conditions, which has been used to effectively remove organosilane thin films from glass surfaces (Figure 1a).[43,44] We find that the binding of gold nanoparticles (AuNPs) significantly hinders the hydrolysis of the silanes beneath the AuNPs (Figure 1b). The AuNPs

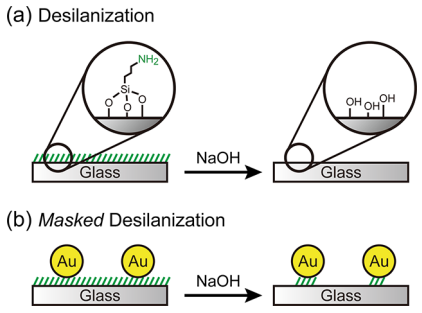

Figure 1. Schematic illustrations of (a) general desilanization and (b) masked desilanization. Aminosilane layers (green lines) are removed by basic hydrolysis. The adsorbed AuNPs (yellow circles) hinder the hydrolysis of the underlying silanes.

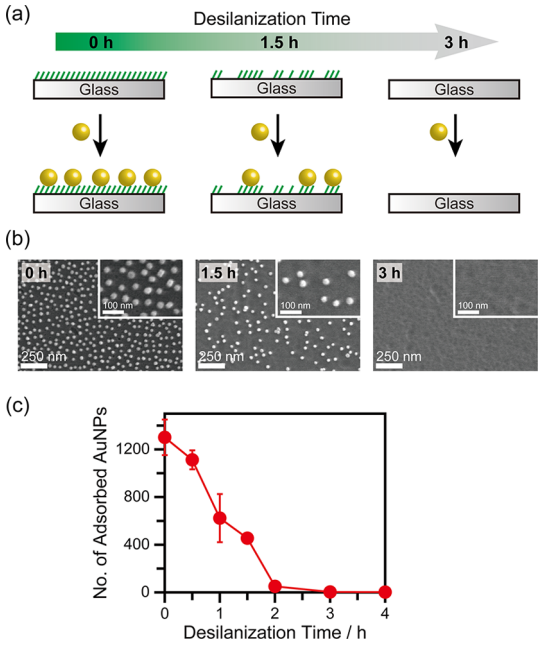

Figure 2. Extent of desilanization of glass slides, as probed by the adsorption of AuNPs. (a) Experimental scheme: as longer reaction time with NaOH (desilanization time) is allowed, more aminosilanes are removed and thus less AuNPs adsorb. (b) Representative SEM images of the AuNPs adsorbed on the aminosilanized glass slides that have reacted with NaOH (1 mM) for 0, 1.5, and 3 h. (c) Changes in the number of adsorbed AuNPs in randomly selected areas (1.73 μm $\times$ 2.56 μm) with increasing desilanization reaction time.

therefore serve as a masking agent for the desilanization reaction.

We measure the (masked) desilanization of glass surfaces through the adsorption and desorption of AuNPs. Citrate-capped AuNPs adsorb well on aminosilanized glass surfaces *via* electrostatic interactions.[45,46] Therefore, the extent of desilanization can be measured by monitoring the change in the number of AuNPs adsorbing on the glass surface after the reaction. First, we prepare aminosilanized glass slides using (3-aminopropyl)trimethoxysilane (APTMS) and let them react with NaOH (1 mM) for periods of time ranging from 0 to 3 h (Figure 2a). The glass slides are

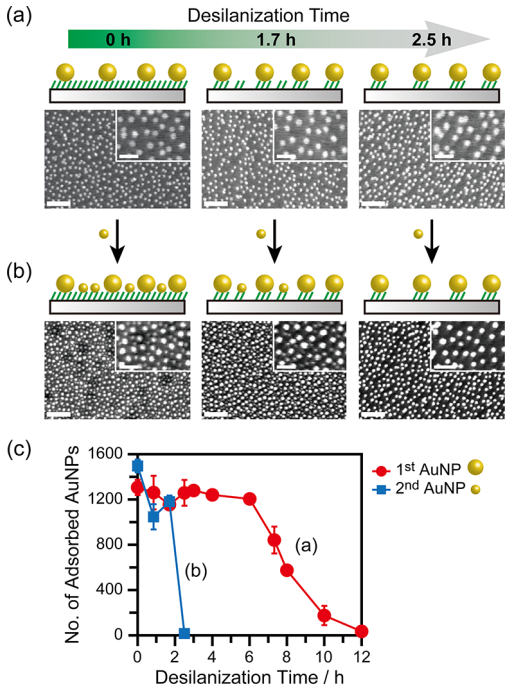

Figure 3. Desilanization of aminosilanized glass slides with AuNPs adsorbed on the surface. (a) SEM images of the AuNP (25 nm)-adsorbed glass slides as they react with NaOH (1 mM) for 0, 1.7, and 2.5 h. (b) SEM images of the AuNP (25 nm)-adsorbed glass slides as they are allowed to adsorb the second AuNPs (15 nm) after the desilanization reaction for 0, 1.7, and 2.5 h. (c) A plot of the number of AuNPs in randomly selected areas (1.73 μm $\times$ 2.56 μm) from (a) and (b). The scale bars in the main and inset images are 250 and 100 nm, respectively.

then immersed in solutions of AuNPs (diameter = 25 $\pm$ 2 nm) for adsorption. The scanning electron microscopy (SEM) images in Figure 2b clearly show that initially the AuNPs adsorb well on the amine-coated glass slides (0 h). As the amine-coated glass slides are treated with NaOH for longer periods of time, the desilanization reaction leaves less aminosilanes on the glass surfaces, leading to the adsorption of fewer amounts of AuNPs. The aminosilane layer is completely removed after 3 h of NaOH treatment, and thus, no AuNPs adsorb on the glass slide (Figure 2c).

The rate of surface desilanization is significantly affected by the presence of AuNPs on the surfaces. For this investigation, we adsorb citrate-capped AuNPs (25 $\pm$ 2 nm, referred to as the first AuNPs here) on the aminosilanized glass surfaces prior to the desilanization reaction. The AuNP-adsorbed glass slides are then reacted with NaOH (1 mM) for different periods of time ranging from 0 to 12 h (Figure 3). As the hydroxides cleave the siloxane bonds between the aminosilanes and the glass surfaces, the AuNPs desorb together with the aminosilanes from the glass surfaces. Contrary to our expectation that all AuNPs would desorb in 3 h, as observed for the bare aminosilanized surfaces in Figure 2, the AuNPs remain adsorbed for up to 6 h of reaction time (Figure 3a and the red line in Figure 3c).

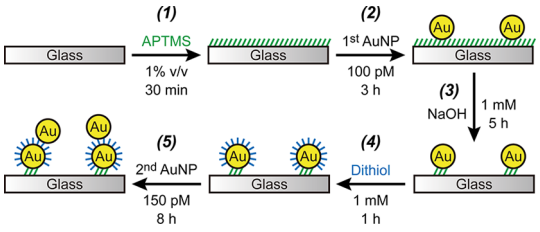

Figure 4. A scheme for stepwise dimer assembly using masked desilanization. (1) Amine coating of glass slides using APTMS, (2) adsorption of the first AuNPs, (3) masked desilanization with NaOH, (4) thiol-functionalization of the first AuNPs, (5) preferential adsorption of the second AuNPs onto the first AuNPs, forming dimers.

This result implies that the aminosilanes under the AuNPs are hydrolyzed by NaOH much more slowly than are free-standing silanes. To examine the state of the free-standing aminosilanes, uncovered by the first AuNPs, we immerse the resulting glass slides in a solution of AuNPs, referred to as the second AuNPs here, with a different size (15 ± 1 nm) from the first AuNPs. The number of the adsorbed second AuNPs decreases with the desilanization reaction time and finally reaches zero after 2.5 h of the reaction, confirming that the aminosilanes unprotected by the first AuNPs follow the normal kinetics of the desilanization reaction (Figure 3b and the blue line in Figure 3c). These observations strongly suggest that the AuNPs bound to the aminosilanes on the glass surfaces protect the underlying silanes from desilanization and therefore serve as *masks*. The citrate-capped AuNPs presumably hinder hydroxides from approaching the silanes immediately underneath the AuNPs due to electrostatic or steric effects.

Assembly of Dimers Using Masked Desilanization. The masked desilanization procedure allows us to prepare homodimers of nanoparticles with a high yield. The idea is that the masked desilanization removes all the aminosilanes from the glass surface except where AuNPs are adsorbed. Then, the subsequently added AuNPs would not adsorb on the glass surface and interact only with the preadsorbed AuNPs if they are appropriately surface-functionalized, leading to the exclusive formation of AuNP dimers without monomers.

Figure 4 illustrates the assembly scheme for the homodimers of nanoparticles. A detailed description of the assembly method is provided in the Methods section. Briefly, the glass slides are thoroughly cleaned and amine-coated using APTMS (step 1). The citrate-capped first AuNPs (25 ± 2 nm) are adsorbed on the glass slides (step 2). We refer to the AuNPs as the first and second AuNPs according to the order in which they are added to the system. The masked desilanization removes the aminosilane layer unprotected by the first AuNPs from the glass surface (step 3). Then, the surfaces of the first AuNPs are modified with thiols using alkanedithiol linkers to enable the attachment of the second AuNPs in the ensuing step (step 4). Finally,

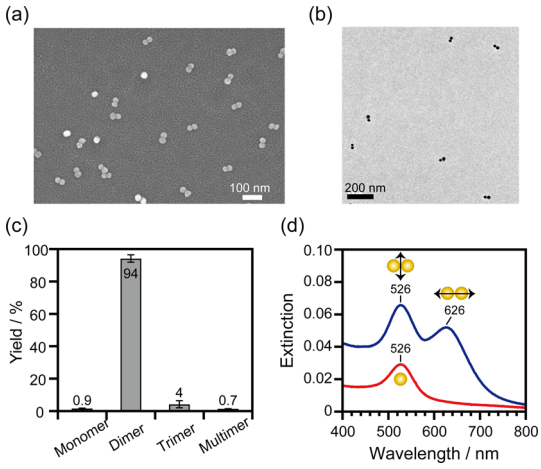

Figure 5. Structural and optical properties of the dimers linked by 1,8-octanedithiol. A representative SEM image of the assemblies formed on a glass slide. (b) A TEM image of the particles desorbed from the glass slide by sonication. (c) Statistics of the assemblies formed on glass slides, measured from the SEM images of five different glass slides (total 607 particles). (d) UV−vis spectrum of dimers (blue curve). For comparison, a UV−vis spectrum of monomers is included (red curve).

the second AuNPs, which are identical to the first AuNPs, are adsorbed onto the first AuNPs *via* the formation of Au−S bonds (step 5). In this step, the second AuNPs do not adsorb on the glass surface due to the absence of the amine functionality following desilanization, leading to a high yield of dimers. The formation of dimers is easily monitored by the visible color change of the glass slide from red to blue arising from the strong plasmon coupling (*vide infra*). After the final step, the dimers on the glass slides are subjected to SEM and UV−vis spectroscopy for structural and plasmonic investigation. Ultrasonication desorbs the AuNP dimers from the glass slides and prepares the dispersed dimers in solutions (see the Methods for details). An aliquot of the solution is sampled for transmission electron microscopy (TEM) measurements.

Figure 5 clearly shows that homodimers of AuNPs are prepared with exceptional purity. Dimers are predominantly observed in the SEM images of the resulting glass slides (Figure 5a). Without the masked desilanization step, a mixture of monomers and dimers is obtained (Supporting Information, Figure S1). Note that the particles that look like monomers in Figure 5a are in fact top views of two stacked particles. These on-top dimers are readily distinguished from monomers by their brighter contrast (Supporting Information, Figure S2). Close inspection of the SEM images also reveals that the dimers are formed on glass slides in various orientations (Supporting Information, Figure S3). TEM images of the dispersed particles also confirm the exclusive formation of dimers (Figure 5b).

We measure the yield from the SEM images of five different glass slides (Figure 5c). Dimers constitute 94 ± 2% of the total 607 particles counted from the

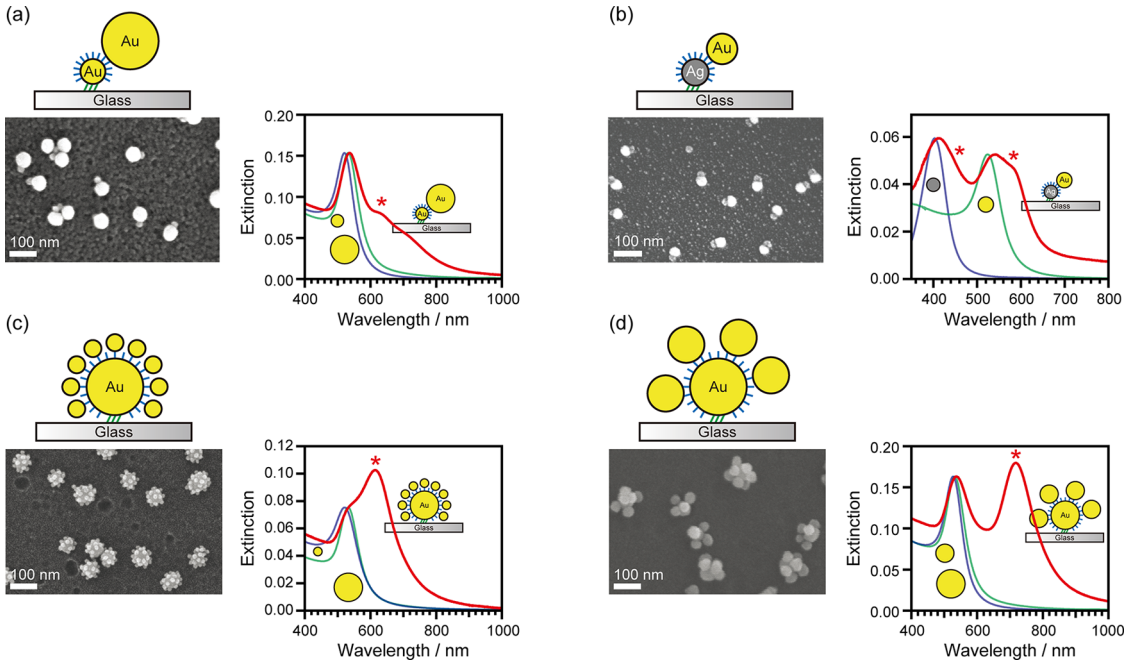

Figure 6. SEM images and UV−vis spectra of various forms of nanoassemblies prepared by the masked desilanization: (a) Au (22 nm)−Au (50 nm) dimers, (b) Ag (18 nm)−Au (25 nm) dimers, (c) Au (50 nm)−Au (12 nm) core−satellite assemblies, and (d) Au (50 nm)−Au (32 nm) clusters. The red curves indicate the UV−vis spectra of the corresponding nanoassemblies. The asterisks mark the plasmon coupling bands. For comparison, the UV−vis spectra of isolated nanoparticles are included with their intensities normalized to the component bands in the assembly spectra (green and blue curves).

images. From the yield and the measured number of the adsorbed first AuNPs, we determine the total number of dimers prepared on one glass slide (25 mm × 12 mm) to be 3 × 10^{10} (Supporting Information). Monomers and multimers (larger than tetramers) are rarely observed. Trimers, apparently formed by a second AuNP bridging two of the first AuNPs in the immediate vicinity, constitute 4 ± 2% of the total particles. The population distribution of the assemblies changes with the concentration of the second AuNP solution. The proportion of trimers increases when we use more concentrated solutions for the second AuNPs in step 5 of the assembly process (Supporting Information, Figure S5). The yield for the dimer also varies with the linkers used in the assembly (Supporting Information, Figure S6). However, slight variations in the yield did not influence the ensemble-averaged properties of dimers (Supporting Information, Figure S7).

Figure 5d presents the optical property of the dimers prepared by the masked desilanization method. The UV−vis extinction spectrum of the dimers linked by 1,8-octanedithiol exhibits two distinct bands, one at 526 nm and the other at 626 nm. The 526 nm band is assigned to the transverse coupling of the surface plasmons in the dimers because it has the same band position as the SPR band of the monomers from step 3 of the assembly process, but with a band intensity almost twice as large. The new band at 626 nm, which is significantly red-shifted from the SPR wavelength of the isolated AuNPs, is most likely due to the longitudinal coupling of the surface plasmons.[35] This band is, therefore, sensitive to the strength of the interaction and the interparticle gap distance (*vide infra*).

Versatility of the New Assembly Method. Our assembly method allows us to modify each step with great flexibility, making it a versatile assembly technique extendable to the preparation of other forms of assemblies beyond homodimers. Using various combinations of nanoparticles with different sizes (12, 22, 32, and 50 nm) and materials (Au and Ag), we successfully prepared size-asymmetric AuNP dimers, Ag−Au heterodimers, core−satellite nanoassemblies, and clusters composed of a few nanoparticles with comparable sizes (Figure 6). The UV−vis spectrum of each assembly shows the distinctive plasmon coupling band, marked by an asterisk. Further analysis of the spectra will be published separately.

The interparticle distance can also be readily tuned by using different linkers in step 4 of the assembly process. The alkanedithiol SAMs formed on the surfaces of the first AuNPs define the interparticle distance between the nanoparticles in the dimers.[47] Therefore, the use of different lengths of alkanedithiols enables the interparticle distance to be finely tuned. Alternatively, other chemical or biological linkers can be used to extend the range of the interparticle distance.

Plasmon Coupling of Dimers with Subnanometer Interparticle Distances. The controllable interparticle distance and ultrahigh purity of the dimers allows us to explore plasmon coupling at the ensemble level as the two nanoparticles approach within the subnanometer

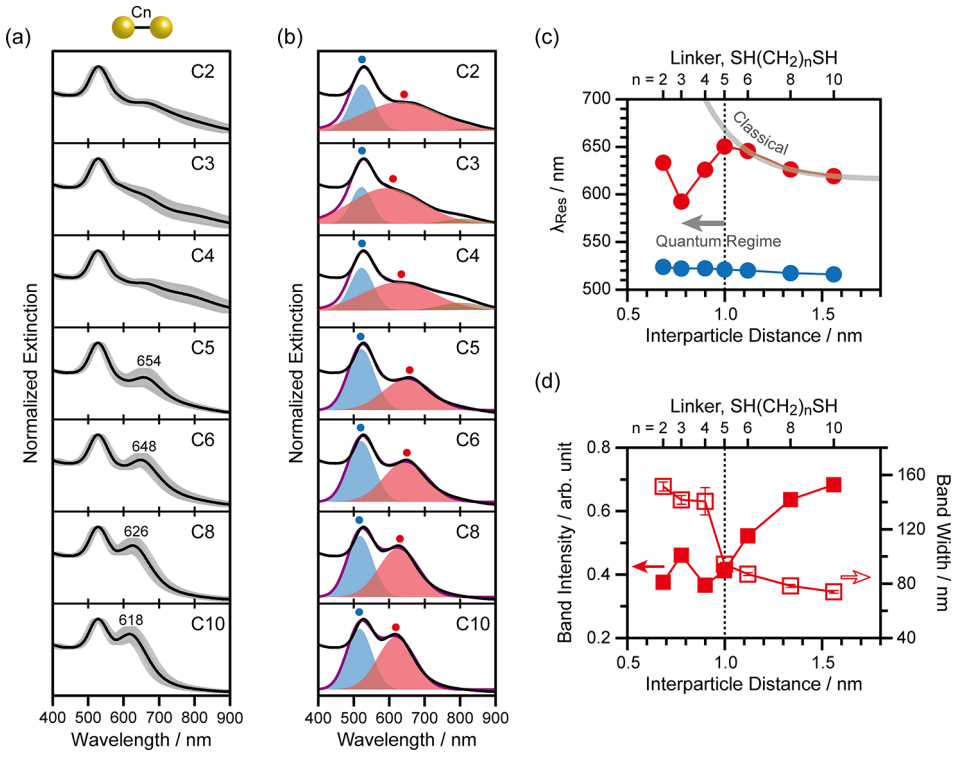

Figure 7. Evolution of the plasmon coupling in AuNP dimers as the interparticle distance is reduced to the subnanometer regime. (a) Averaged UV−vis spectra of AuNP dimers linked by alkanedithiol, $SH(CH_2)_nSH$ (abbreviated as Cn), based on 10 experiments. The gray lines represent one standard deviation. (b) Decomposition of the UV−vis spectra of the AuNP dimers using Gaussian functions. The purple curves indicate the reproduced spectra from the best fit between 490 and 900 nm. The red and blue dots mark the peak wavelengths of the major Gaussian components. The UV−vis spectra of the dimers with C4 to C2 linkers have an extra Gaussian component in the near IR region, although the intensity is very small (brown curve). (c) A plot of the resonance wavelengths of the plasmon coupling bands (red and blue dots in (b)) as a function of the interparticle distance. The gray curve is the best fit to an exponential function, representing the classical electromagnetic model for plasmon coupling. The vertical dotted line marks an interparticle distance of 1 nm, where quantum plasmon coupling appears to begin. (d) Plots of the intensity (filled squares) and width (open squares) of the longitudinal plasmon coupling band (red curve in (b)) as a function of the interparticle distance.

range. We changed the interparticle distance from 0.7 to 1.6 nm by using a series of alkanedithiol linkers, $SH(CH_2)_nSH$ (n = 2−10; abbreviated as Cn hereafter). Figure 7a shows the optical response of the resulting dimers. For each linker, we acquired UV−vis spectra from 10 independently prepared samples, normalized the intensity with respect to the intensity of the 526 nm band, and averaged them. The gray lines in Figure 7a represent one standard deviation. The most noticeable spectral change as the shorter linker is used (from C10 to C5) is the redshift in the longitudinal surface plasmon coupling band (from 618 to 654 nm). This redshift is consistent with previous theoretical and experimental results.[14−24] As the interparticle distance decreases, the interaction between the two nanoparticles strengthens, lowering the bonding dipole plasmon mode. The continuing redshift of the plasmon coupling band with decreasing interparticle distance, however, drastically changes when the interparticle gap narrows to within 1 nm. The UV−vis spectra of the AuNP dimers linked by C4, C3, and C2 significantly broaden such that the surface plasmon coupling band is no longer distinguishable.

To reveal the underlying features, we decomposed the spectra with Gaussian functions (see the Methods for details). The UV−vis spectra of the AuNP dimers with C10 to C5 linkers are fitted with two Gaussian functions, each representing the transverse (blue curve) and longitudinal (red curve) plasmon coupling band (Figure 7b). The UV−vis spectra of the C4- to C2-linked dimers are fitted with three Gaussians to make the fitting converge properly, resulting in an extra component in the near IR region with a very small intensity (brown curve) in addition to the two major Gaussian components (blue and red curves). The evolution of the major components in Figure 7b clearly shows that the longitudinal coupling band gradually redshifts as the linker shortens from C10 to C5 and suddenly broadens for C4−C2, reflecting the overall spectral features.

We plotted the changes in the plasmon coupling bands as a function of the interparticle distance in Figure 7c,d for further analysis. The interparticle distance was calculated based on the SAM structures of alkanedithiol using density functional theory (DFT).[42,47] We note that it is extremely difficult to measure such short interparticle distances reliably using high-resolution

TEM due to the structural deformation caused by repeated exposure to the electron beam (Supporting Information, Figure S8).[48−51] Figure 7c shows that the resonance wavelength (λ_{Res}) of the longitudinal plasmon coupling band redshifts as the interparticle distance decreases down to ∼1 nm, whereas the transverse plasmon coupling band is largely independent of the interparticle distance. The redshift fits well to an exponential function (or a power function), consistent with the classical electrodynamics model (gray line).[15,22−24,52] Near ∼1 nm (marked by the vertical dotted line), however, the shift begins to deviate from the classical model. The redshift lessens and switches over to a blueshift as the interparticle gap further narrows. The band intensity and the width also abruptly change at ∼1 nm (Figure 7d). The intensity of the plasmon coupling band continually diminishes until the interparticle distance reaches ∼1 nm, at which the width of the band significantly increases.

Those spectral features that we observed strongly indicate that quantum effects play a significant role in the optical response of AuNP dimers with subnanometer interparticle distances. Quantum mechanical calculations by Nordlander and co-workers revealed that electron tunneling between the nanoparticles leads to two important effects.[25,26] One is that the plasmon coupling band redshifts by smaller amounts than is predicted by classical electromagnetic theory and with diminished intensity. The electron tunneling across the junction effectively screens the plasmonic interactions. The reduced electromagnetic interactions between the two nanoparticles then lead to a smaller hybridization and thus a smaller redshift and intensity of the plasmon coupling band. The other is that electron tunneling creates new modes, denoted as charge transfer plasmons (CTPs). The lowest energy CTP mode usually appears in the IR region, particularly when the nanoparticles are in contact. Higher-order CTP modes have shorter resonance wavelengths. Notably, a second CTP mode (CTP′) appears at a slightly shorter wavelength of the bonding dipolar plasmon coupling band in the quantum regime.[25,26,29] The CTP′ band then gains its intensity and blueshifts as the interparticle distance is reduced. The CTP′ band is also significantly broader than the classical plasmon coupling band due to the dissipation of the electron current across the high resistance region at the junction.[26]

The observed spectral patterns in Figure 7 conform to the theoretical description of the signatures arising from the quantum effects. We observed that the plasmon coupling band gradually decreases in intensity as the two nanoparticles approach the tunneling regime (C10−C5 in Figure 7b). A new band then appears at a blueshifted wavelength with a significantly broadened bandwidth with respect to the plasmon coupling band (C4 in Figure 7b). This new band, attributed to the CTP′ mode, then blueshifts as the interparticle distance decreases in the quantum regime (C4−C2 in Figure 7b,c). These results consistently indicate that the quantum plasmon resonances occur in the AuNP dimers. Our ensemble measurements also agree with previous single-particle level measurements using atomic force microscopy (AFM) and electron energy loss spectroscopy (EELS).[27,29] Baumberg and co-workers similarly observed a transition in the coupling band from a redshift to a blueshift as quantum tunneling began to dominate the plasmon interactions across subnanometer cavities.[27] For a silver nanoparticle dimer with its interparticle distance dynamically controlled by the irradiation of the electron beam in a scanning TEM (STEM), Dionne and coworkers observed the CTP′ band at separations below ∼0.5 nm.[29]

Comparison with previous theoretical and experimental studies confirms that quantum effects do influence the plasmonic response of AuNP dimers in the subnanometer interparticle distance regime. A few spectral features of the dimers in the quantum coupling regime, such as the anomalous band position of the C2-linked dimers and the long wavelength component, albeit small, in the spectra of the C3- and C4-linked dimers, remain elusive at this stage. As Nordlander and co-workers indicated, the energy and width of the CTP resonance depend sensitively on the details of the quantum coupling such as the touching profile and the electron density at the junction.[25] A fine balance between the conductance at the junction (that leads to blueshifts) and the electron density from the local structure of metal nanoparticles (that leads to redshifts) could cause the deviation between theory and experiment. Another possibility is that the lowest energy CTP mode has been blueshifted from the IR region as the interparticle distance decreases in the quantum regime and might appear as the resonance band of the C2-linked dimers. Although feasible, however, this requires a significantly large shift of the lowest energy CTP. Further comparative studies with quantum mechanical calculations on the specific dimer systems used in this experiment will provide a more complete understanding of the observed spectra and quantum plasmon coupling.

Another intriguing issue is at which distance the quantum plasmon resonances begin to occur. Our experimental results suggest that electron tunneling begins to influence the plasmon resonances at an interparticle distance of ∼1 nm for the AuNP dimers. In contrast, Duan *et al.* report that no quantum effect has been observed down to the gap size of ∼0.5 nm in the nanoprism pairs fabricated by the state-of-the-art lithography.[53] It is possible that our DFT calculations based on the SAM structures of alkanedithiols consistently overestimate the interparticle distances, which would shift the onset distance for the quantum plasmon resonances to a longer distance than the true

value.[42] On the other hand, one should also consider that the AuNPs in our experiments are connected by molecular linkers. A recent study by Tan *et al.* reveals that the presence of the molecules with the favorable electronic structures for tunneling extends the onset gap distance for the quantum effects to ~1.3 nm.[30] These results indicate that the electronic structures of the bridging molecules as well as the shape and the area of the junctions play an important role in quantum tunneling between the plasmonic resonators. Exploration of the through-bond tunneling effect on the optical resonance spectra of the AuNP dimers using aromatic dithiol linkers is currently in progress in our laboratory.

CONCLUSIONS

We developed a highly efficient and facile assembly method for the preparation of dimers and other forms of nanoassemblies. The AuNPs adsorbed on silanized glass slides served as masking agents for desilanization. This masked desilanization allowed us to prepare AuNP dimers on glass slides in a controlled fashion with remarkably high yields (~90%). The resulting AuNP dimers exhibited strong surface plasmon coupling, which redshifted in energy with decreasing interparticle distances. When the interparticle distance was reduced to the subnanometer range, the plasmon coupling band began to blueshift and drastically broadened, suggesting that quantum tunneling significantly influenced the plasmon coupling in this distance regime. Our new assembly method is widely applicable to the production of many forms of nanoassemblies, through which it will contribute to the fundamental understanding of plasmonic interactions between nanoparticles in close proximity and thereby advance the applications of plasmonic nanoassemblies.

METHODS

Chemicals. All chemicals used for the synthesis and assembly of nanoparticles were purchased and used without further purification. The list of compounds and their purities is available in the Supporting Information.

Preparation and Characterization of Nanoparticles. We adopted the Turkevich and the seeded growth method to prepare citrate-capped AuNPs with diameters of 12, 15, 22, 25, 32, and 50 nm.[54,55] The seed AuNPs (14.9 ± 1.3 nm), synthesized by the reduction of Au^{3+} with citrate, were grown to the desired sizes by adding appropriate amounts of growth solutions ($HAuCl_4$ and sodium citrate) and adjusting the reaction time. The detailed reaction conditions for each AuNP are listed in the Supporting Information and in a previous publication.[42] AgNPs (18 nm) were purchased from Ted Pella, Inc. The sizes of the nanoparticles were measured using TEM (JEOL JEM-2100F). Characterization data for each AuNP are summarized in the Supporting Information (Table S1).

Aminosilanization of Glass Slides. Glass slides were coated with amine groups through silanization to enable the adsorption of citrate-capped AuNPs.[45,56,57] Glass slides (25 mm × 12 mm, Marienfeld, Germany) were cleaned in a 15% RBS detergent solution at 90 °C and treated with a solution of HCl and methanol (1:1 v/v) for 30 min. After a drying step in an oven at 100 °C for 3 h, the glass slides were immersed in an ethanol solution of APTMS (1% v/v) for 30 min for aminosilanization. The aminosilanization of the glass surfaces was completed by washing with ethanol, sonicating in ethanol for 5 min, and drying in an oven at 120 °C for 3 h.

Adsorption of AuNPs on Amine-Coated Glass Slides. AuNPs were adsorbed on glass slides by immersing the aminosilanized glass slides in an aqueous solution of citrate-capped AuNPs.[45,56,57] The initially transparent glass slides turned red upon the adsorption of the AuNPs. The density of the adsorbed AuNPs on the glass slide depended on the concentration of AuNPs and the immersion time. We probed the adsorbed AuNPs on the glass slides using SEM (Hitachi S-4300, S-4800, or Carl Zeiss Supra 55).

Desilanization of Glass Slides Using NaOH. The aminosilane layers on the glass slides were removed by a desilanization reaction in which the silanes were hydrolyzed under basic conditions.[43,44] For the reaction, the aminosilanized glass slides were immersed in solutions of NaOH. The extent of desilanization critically depends on the reaction time and the concentration of NaOH. We measured the extent of desilanization by probing the number of AuNPs that adsorbed to the glass slides after the desilanization reaction using SEM. To explore the effect of the reaction time, we immersed the aminosilanized glass slides in 1 mL of NaOH solution for periods of time ranging from 0 to 4 h. After washing with deionized water, we then placed the glass slides in a solution of AuNPs (650 pM, 5 mL) for 4 h. SEM measurements of the number of adsorbed AuNPs in randomly selected areas (1.73 μm × 2.56 μm) revealed the extent of desilanization (Figure 2). We also explored the effect of the concentration of NaOH (Supporting Information, Figure S10).

Masked Desilanization. We found that the AuNPs adsorbed on the aminosilanized glass slides protected the silanes underneath the particles from the desilanization reaction. We prepared aminosilanized glass slides and adsorbed AuNPs (25 nm) using the procedure described above. Then, the AuNP-adsorbed glass slides were immersed in a NaOH solution (1 mM, 5 mL) for 0−12 h. The removal of the silanes under the AuNPs was measured using SEM by examining desorption of the AuNPs (Figure 3a). The extent of desilanization in unprotected areas was measured by adsorbing the second AuNPs (15 nm, 2.5 nM, 5 mL) for 4 h. The number of second AuNPs adsorbed on the glass slides was measured in randomly selected areas (1.73 μm × 2.56 μm) using SEM (Figure 3b).

Dimer Assembly. Dimers were assembled on glass slides in the following steps. Between each step, the glass slides were washed with the solvent used in the prior step and then rinsed with a solvent to be used in the ensuing step. **Step 1: Silanization**. Glass slides were amine-coated through silanization with APTMS. Cleaned glass slides were immersed in an ethanol solution of APTMS (1% v/v, 5 mL) for 30 min, rinsed with ethanol by sonication for 5 min, and dried in an oven at 120 °C for 3 h. **Step 2: Adsorption of the first AuNPs.** The first AuNPs (25 nm) were adsorbed on the amine-coated glass slides. Incubation of the amine-coated glass slides in the AuNP solution (100 pM, 5 mL) for 3 h led to the adsorption of the AuNPs. **Step 3: Masked desilanization.** All amine functional groups were removed from the glass surface except for those binding the first AuNPs. The AuNP-adsorbed glass slides were placed in a NaOH solution (1 mM, 5 mL) for 5 h. **Step 4: Thiol-functionalization of the first AuNPs.** To attach the second AuNPs in step 5, the surfaces of the first AuNPs were modified with thiols. The AuNP-adsorbed glass slides from step 3 were immersed in a 1,8-octanedithiol solution in ethanol (1 mM, 5 mL) for 1 h. **Step 5: Adsorption of the second AuNPs.** The citrate-capped second AuNPs (25 nm) bound to the thiol-functionalized first AuNPs, forming dimers on the glass slide. Note that the second AuNPs did not adsorb on the glass slides because the amine functional groups had been removed from the glass surface in step 3. The glass slides were immersed in the AuNP solution (150 pM, 5 mL) for 8 h.

The above steps were used to prepare dimers on the glass slides. To prepare dimers dispersed in solution, we imparted additional electrostatic stability to the dimers by coating the dimer surface with carboxylate-terminated SAMs. The dimer-formed glass slides were immersed in 11-mercaptoundecanoic acid (MUA) in EtOH (1 mM, 5 mL) for 1 h. After washing with ethanol, we sonicated the slides in ethanol containing MUA (10 μM, 5 mL) for 30 s to desorb the dimers into the solution.

To measure the surface plasmon coupling as a function of interparticle distance, we assembled dimers with a series of alkanedithiols, from C2 to C10, in step 4. The resulting dimers on glass slides were subjected to UV−vis spectroscopy. The glass slides were immersed in ethanol during the measurements to avoid the aggregation of particles from the drying effect.

Fitting of a Spectrum with Gaussian Functions. The UV−vis spectra for the dimers with C4 to C2 linkers, although no obvious resolvable peaks are found, clearly have the structures such as shoulders and humps. We attempted to resolve those structures by fitting them with Gaussian functions and thereby derive useful information. We performed the fitting using Igor Pro (ver. 6.3.2.3). The fitting range was set at 490−900 nm to exclude the continuum interband transition of AuNPs in the UV region. All other fitting parameters, such as the position, width, and amplitude of a Gaussian function, were allowed to run free to fit the spectra the best. We made sure that the fitting converged properly and yielded consistent results for slightly different initial guesses. We tried to reproduce the overall spectra by fitting them with the minimum possible number of Gaussian functions.

Conflict of Interest: The authors declare no competing financial interest.

Supporting Information Available: Control experiment for the effect of the masked desilanization on high yield preparation of dimers, distinction between on-top dimers and monomers in SEM images, the orientation of the dimers on glass slides observed in SEM images, quantification of the number of AuNP dimers on a glass slide, an increase of trimers with the concentration of the second AuNPs, dimer yields for different linkers, effect of the slight variations in the yield on ensemble-averaged properties, measurements of interparticle distances using HRTEM, preparation and characterization of nanoparticles, and effect of the concentration of NaOH on desilanization. This material is available free of charge *via* the Internet at http://pubs.acs.org.

Acknowledgment. This research was supported by the Basic Science Research Program through the National Research Foundation of Korea (NRF) funded by the Ministry of Education (2013R1A1A2008336).

REFERENCES AND NOTES

1. Odom, T. W.; Schatz, G. C. Introduction to Plasmonics. *Chem. Rev.* **2011**, *111*, 3667–3668.
2. Jain, P. K.; Huang, X.; El-Sayed, I. H.; El-Sayed, M. A. Noble Metals on the Nanoscale: Optical and Photothermal Properties and Some Applications in Imaging, Sensing, Biology, and Medicine. *Acc. Chem. Res.* **2008**, *41*, 1578–1586.
3. Mayer, K. M.; Hafner, J. H. Localized Surface Plasmon Resonance Sensors. *Chem. Rev.* **2011**, *111*, 3828–3857.
4. Huang, X.; El-Sayed, I. H.; Qian, W.; El-Sayed, M. A. Cancer Cell Imaging and Photothermal Therapy in the Near-Infrared Region by Using Gold Nanorods. *J. Am. Chem. Soc.* **2006**, *128*, 2115–2120.
5. Linic, S.; Christopher, P.; Ingram, D. B. Plasmonic-Metal Nanostructures for Efficient Conversion of Solar to Chemical Energy. *Nat. Mater.* **2011**, *10*, 911–921.
6. Loo, C.; Lowery, A.; Halas, N.; West, J.; Drezek, R. Immunotargeted Nanoshells for Integrated Cancer Imaging and Therapy. *Nano Lett.* **2005**, *5*, 709–711.
7. Kelly, K. L.; Coronado, E.; Zhao, L. L.; Schatz, G. C. The Optical Properties of Metal Nanoparticles: The Influence of Size, Shape, and Dielectric Environment. *J. Phys. Chem. B* **2003**, *107*, 668–677.
8. Rycenga, M.; Cobley, C. M.; Zeng, J.; Li, W.; Moran, C. H.; Zhang, Q.; Qin, D.; Xia, Y. Controlling the Synthesis and Assembly of Silver Nanostructures for Plasmonic Applications. *Chem. Rev.* **2011**, *111*, 3669–3712.
9. Halas, N. J.; Lal, S.; Chang, W.-S.; Link, S.; Nordlander, P. Plasmons in Strongly Coupled Metallic Nanostructures. *Chem. Rev.* **2011**, *111*, 3913–3961.
10. Talley, C. E.; Jackson, J. B.; Oubre, C.; Grady, N. K.; Hollars, C. W.; Lane, S. M.; Huser, T. R.; Nordlander, P.; Halas, N. J. Surface-Enhanced Raman Scattering from Individual Au Nanoparticles and Nanoparticle Dimer Substrates. *Nano Lett.* **2005**, *5*, 1569–1574.
11. Rycenga, M.; Camargo, P. H. C.; Li, W.; Moran, C. H.; Xia, Y. Understanding the SERS Effects of Single Silver Nanoparticles and Their Dimers, One at a Time. *J. Phys. Chem. Lett.* **2010**, *1*, 696–703.
12. Xie, W.; Walkenfort, B.; Schlücker, S. Label-Free SERS Monitoring of Chemical Reactions Catalyzed by Small Gold Nanoparticles Using 3D Plasmonic Superstructures. *J. Am. Chem. Soc.* **2013**, *135*, 1657–1660.
13. Zhang, J.; Fu, Y.; Chowdhury, M. H.; Lakowicz, J. R. Metal-Enhanced Single-Molecule Fluorescence on Silver Particle Monomer and Dimer: Coupling Effect between Metal Particles. *Nano Lett.* **2007**, *7*, 2101–2107.
14. Rechberger, W.; Hohenau, A.; Leitner, A.; Krenn, J. R.; Lamprecht, B.; Aussenegg, F. R. Optical Properties of Two Interacting Gold Nanoparticles. *Opt. Commun.* **2003**, *220*, 137–141.
15. Gunnarsson, L.; Rindzevicius, T.; Prikulis, J.; Kasemo, B.; Käll, M.; Zou, S.; Schatz, G. C. Confined Plasmons in Nanofabricated Single Silver Particle Pairs: Experimental Observations of Strong Interparticle Interactions. *J. Phys. Chem. B* **2005**, *109*, 1079–1087.
16. Jain, P. K.; Huang, W.; El-Sayed, M. A. On the Universal Scaling Behavior of the Distance Decay of Plasmon Coupling in Metal Nanoparticle Pairs: A Plasmon Ruler Equation. *Nano Lett.* **2007**, *7*, 2080–2088.
17. Reinhard, B. M.; Siu, M.; Agarwal, H.; Alivisatos, A. P.; Liphardt, J. Calibration of Dynamic Molecular Rulers Based on Plasmon Coupling between Gold Nanoparticles. *Nano Lett.* **2005**, *5*, 2246–2252.
18. Sheikholeslami, S.; Jun, Y.-W.; Jain, P. K.; Alivisatos, A. P. Coupling of Optical Resonances in a Compositionally Asymmetric Plasmonic Nanoparticle Dimer. *Nano Lett.* **2010**, *10*, 2655–2660.
19. Su, K.-H.; Wei, Q.-H.; Zhang, X.; Mock, J. J.; Smith, D. R.; Schultz, S. Interparticle Coupling Effects on Plasmon Resonances of Nanogold Particles. *Nano Lett.* **2003**, *3*, 1087–1090.
20. Prodan, E.; Radloff, C.; Halas, N. J.; Nordlander, P. A Hybridization Model for the Plasmon Response of Complex Nanostructures. *Science* **2003**, *302*, 419–422.
21. Nordlander, P.; Oubre, C.; Prodan, E.; Li, K.; Stockman, M. I. Plasmon Hybridization in Nanoparticle Dimers. *Nano Lett.* **2004**, *4*, 899–903.
22. Hill, R. T.; Mock, J. J.; Hucknall, A.; Wolter, S. D.; Jokerst, N. M.; Smith, D. R.; Chilkoti, A. Plasmon Ruler with Angstrom Length Resolution. *ACS Nano* **2012**, *6*, 9237–9246.
23. Yoon, J. H.; Yoon, S. Probing Interfacial Interactions Using Core-Satellite Plasmon Rulers. *Langmuir* **2013**, *29*, 14772–14778.
24. Yang, L.; Wang, H.; Yan, B.; Reinhard, B. M. Calibration of Silver Plasmon Rulers in the 1−25 nm Separation Range: Experimental Indications of Distinct Plasmon Coupling Regimes. *J. Phys. Chem. C* **2010**, *114*, 4901–4908.
25. Zuloaga, J.; Prodan, E.; Nordlander, P. Quantum Description of the Plasmon Resonances of a Nanoparticle Dimer. *Nano Lett.* **2009**, *9*, 887–891.
26. Esteban, R.; Borisov, A. G.; Nordlander, P.; Aizpurua, J. Bridging Quantum and Classical Plasmonics with a Quantum-Corrected Model. *Nat. Commun.* **2012**, *3*, 825.
27. Savage, K. J.; Hawkeye, M. M.; Esteban, R.; Borisov, A. G.; Aizpurua, J.; Baumberg, J. J. Revealing the Quantum Regime in Tunnelling Plasmonics. *Nature* **2012**, *491*, 574–577.
28. Yoon, J. H.; Zhou, Y.; Blaber, M. G.; Schatz, G. C.; Yoon, S. Surface Plasmon Coupling of Compositionally Heterogeneous Core-Satellite Nanoassemblies. *J. Phys. Chem. Lett.* **2013**, *4*, 1371–1378.

29. Scholl, J. A.; García-Etxarri, A.; Koh, A. L.; Dionne, J. A. Observation of Quantum Tunneling between Two Plasmonic Nanoparticles. *Nano Lett.* **2013**, *13*, 564–569.
30. Tan, S. F.; Wu, L.; Yang, J. K. W.; Bai, P.; Bosman, M.; Nijhuis, C. A. Quantum Plasmon Resonances Controlled by Molecular Tunnel Junctions. *Science* **2014**, *343*, 1496–1499.
31. Alivisatos, A. P.; Johnsson, K. P.; Peng, X.; Wilson, T. E.; Loweth, C. J.; Bruchez, M. P.; Schultz, P. G. Organization of 'Nanocrystal Molecules' Using DNA. *Nature* **1996**, *382*, 609–611.
32. Chen, G.; Wang, Y.; Tan, L. H.; Yang, M.; Tan, L. S.; Chen, Y.; Chen, H. High-Purity Separation of Gold Nanoparticle Dimers and Trimers. *J. Am. Chem. Soc.* **2009**, *131*, 4218–4219.
33. Wang, Y.; Chen, G.; Yang, M.; Silber, G.; Xing, S.; Tan, L. H.; Wang, F.; Feng, Y.; Liu, X.; Li, S.; *et al.* A Systems Approach towards the Stoichiometry-Controlled Hetero-Assembly of Nanoparticles. *Nat. Commun.* **2010**, *1*, 87.
34. Busson, M. P.; Rolly, B.; Stout, B.; Bonod, N.; Larquet, E.; Polman, A.; Bidault, S. Optical and Topological Characterization of Gold Nanoparticle Dimers Linked by a Single DNA Double Strand. *Nano Lett.* **2011**, *11*, 5060–5065.
35. Thacker, V. V.; Herrmann, L. O.; Sigle, D. O.; Zhang, T.; Liedl, T.; Baumberg, J. J.; Keyser, U. F. DNA Origami Based Assembly of Gold Nanoparticle Dimers for Surface-Enhanced Raman Scattering. *Nat. Commun.* **2014**, *5*, 3448.
36. Sardar, R.; Heap, T. B.; Shumaker-Parry, J. S. Versatile Solid Phase Synthesis of Gold Nanoparticle Dimers Using an Asymmetric Functionalization Approach. *J. Am. Chem. Soc.* **2007**, *129*, 5356–5357.
37. Xu, X.; Rosi, N. L.; Wang, Y.; Huo, F.; Mirkin, C. A. Asymmetric Functionalization of Gold Nanoparticles with Oligonucleotides. *J. Am. Chem. Soc.* **2006**, *128*, 9286–9287.
38. Tan, L. H.; Xing, H.; Chen, H.; Lu, Y. Facile and Efficient Preparation of Anisotropic DNA-Functionalized Gold Nanoparticles and Their Regioselective Assembly. *J. Am. Chem. Soc.* **2013**, *135*, 17675–17678.
39. Lim, D.-K.; Jeon, K.-S.; Kim, H. M.; Nam, J.-M.; Suh, Y. D. Nanogap-Engineerable Raman-Active Nanodumbbells for Single-Molecule Detection. *Nat. Mater.* **2010**, *9*, 60–67.
40. Hu, Y.; Sun, Y. A Generic Approach for the Synthesis of Dimer Nanoclusters and Asymmetric Nanoassemblies. *J. Am. Chem. Soc.* **2013**, *135*, 2213–2221.
41. Yim, T. J.; Wang, Y.; Zhang, X. Synthesis of a Gold Nanoparticle Dimer Plasmonic Resonator through Two-Phase-Mediated Functionalization. *Nanotechnology* **2008**, *19*, 435605.
42. Yoon, J. H.; Lim, J.; Yoon, S. Controlled Assembly and Plasmonic Properties of Asymmetric Core-Satellite Nanoassemblies. *ACS Nano* **2012**, *6*, 7199–7208.
43. Locascio-Brown, L.; Plant, A. L.; Durst, R. A.; Brizgys, M. V. Radiometric and Fluorometric Determination of Aminosilanes and Protein Covalently Bound to Thermally Pretreated Glass Surfaces. *Anal. Chim. Acta* **1990**, *228*, 107–116.
44. Iler, R. K. *The Chemistry of Silica: Solubility, Polymerization, Colloid and Surface Properties and Biochemistry of Silica*; Wiley: New York, 1979.
45. Freeman, R. G.; Grabar, K. C.; Allison, K. J.; Bright, R. M.; Davis, J. A.; Guthrie, A. P.; Hommer, M. B.; Jackson, M. A.; Smith, P. C.; Walter, D. G.; *et al.* Self-Assembled Metal Colloid Monolayers: An Approach to SERS Substrates. *Science* **1995**, *267*, 1629–1632.
46. Grabar, K. C.; Freeman, R. G.; Hommer, M. B.; Natan, M. J. Preparation and Characterization of Au Colloid Monolayers. *Anal. Chem.* **1995**, *67*, 735–743.
47. Love, J. C.; Estroff, L. A.; Kriebel, J. K.; Nuzzo, R. G.; Whitesides, G. M. Self-Assembled Monolayers of Thiolates on Metals as a Form of Nanotechnology. *Chem. Rev.* **2005**, *105*, 1103–1169.
48. Jose-Yacaman, M.; Gutierrez-Wing, C.; Miki, M.; Yang, D.-Q.; Piyakis, K. N.; Sacher, E. Surface Diffusion and Coalescence of Mobile Metal Nanoparticles. *J. Phys. Chem. B* **2005**, *109*, 9703–9711.
49. Chen, Y.; Palmer, R. E.; Wilcoxon, J. P. Sintering of Passivated Gold Nanoparticles under the Electron Beam. *Langmuir* **2006**, *22*, 2851–2855.
50. Lim, T. H.; McCarthy, D.; Hendy, S. C.; Stevens, K. J.; Brown, S. A.; Tilley, R. D. Real-Time TEM and Kinetic Monte Carlo Studies of the Coalescence of Decahedral Gold Nanoparticles. *ACS Nano* **2009**, *3*, 3809–3813.
51. Wustholz, K. L.; Henry, A.-I.; McMahon, J. M.; Freeman, R. G.; Valley, N.; Piotti, M. E.; Natan, M. J.; Schatz, G. C.; Van Duyne, R. P. Structure-Activity Relationships in Gold Nanoparticle Dimers and Trimers for Surface-Enhanced Raman Spectroscopy. *J. Am. Chem. Soc.* **2010**, *132*, 10903–10910.
52. Huang, F. M.; Wilding, D.; Speed, J. D.; Russel, A. E.; Bartlett, P. N.; Baumberg, J. J. Dressing Plasmons in Particle-in-Cavity Architectures. *Nano Lett.* **2011**, *11*, 1221–1226.
53. Duan, H.; Fernández-Domínguez, A. I.; Bosman, M.; Maier, S. A.; Yang, J. K. W. Nanoplasmonics: Classical Down to the Nanometer Scale. *Nano Lett.* **2012**, *12*, 1683–1689.
54. Bastús, N. G.; Comenge, J.; Puntes, V. Kinetically Controlled Seeded Growth Synthesis of Citrate-Stabilized Gold Nanoparticles of up to 200 nm: Size Focusing *versus* Ostwald Ripening. *Langmuir* **2011**, *27*, 11098–11105.
55. Turkevich, J.; Stevenson, P. C.; Hillier, J. A Study of the Nucleation and Growth Processes in the Synthesis of Colloidal Gold. *Discuss. Faraday Soc.* **1951**, *11*, 55–75.
56. Musick, M. D.; Keating, C. D.; Lyon, L. A.; Botsko, S. L.; Peña, D. J.; Holliway, W. D.; McEvoy, T. M.; Richardson, J. N.; Natan, M. J. Metal Films Prepared by Stepwise Assembly. 2. Construction and Characterization of Colloidal Au and Ag Multilayers. *Chem. Mater.* **2000**, *12*, 2869–2881.
57. Nath, N.; Chilkoti, A. Label-Free Biosensing by Surface Plasmon Resonance of Nanoparticles on Glass: Optimization of Nanoparticle Size. *Anal. Chem.* **2004**, *76*, 5370–5378.